Inorganic Chemistry

pubs.acs.org/IC
Article

Reversible Redox Ligand-Centered Reactivity in 2,6-Bisiminopyridine Aluminum Systems

Juan Manuel Delgado-Collado,[§] Hellen Videa,[§] Pablo J. Serrano-Laguna,[§] M. Ángeles Fuentes, Eleuterio Álvarez, Antonio Díaz Quintana, Antonio J. Martínez-Martínez,* Antonio Rodríguez-Delgado,* and Juan Cámpora*

Cite This: *Inorg. Chem.* 2024, 63, 19156−19166

Read Online

ACCESS | Metrics & More | Article Recommendations | Supporting Information

ABSTRACT: We report the synthesis of cationic 2,6-bisiminopyridine organoaluminum complexes, $[(BIP)AlR_2]^+$, as stable $BAr^F{}_4^-$ or PF_6^- salts, and their reversible single-electron reduction into well-defined paramagnetic species, $[(BIP\cdot)AlR_2]$. Four redox couples, $[(BIP)AlR_2]^{+/0}$, have been fully characterized through structural, spectroscopic, electrochemical and computational techniques.

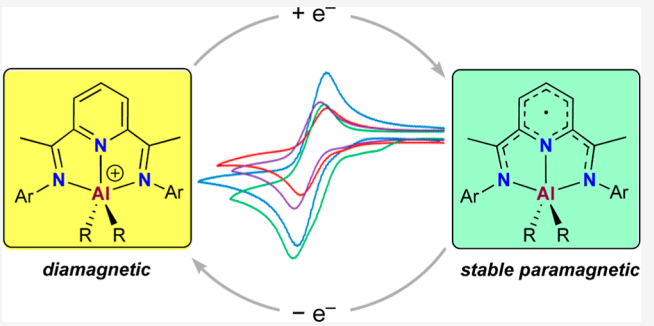

INTRODUCTION

Replacing costly or scarce chemical elements with more abundant alternatives is essential for advancing sustainable technologies.[1] This task is particularly challenging for catalysts based on noble metals since these facilitate various bond formation/cleavage reactions through facile and reversible two-electron redox processes—a capability not easily replicated by more abundant metals.[2,3] While many artificial catalysts rely on these scarce precious metals, living organisms employ enzymes containing "base" metals like Fe or Cu and, frequently, main-group elements like Zn or Mg that lack inherent redox capabilities.[4] In these biological systems, the organic ligand framework is crucial for enabling electron, proton, or even complex molecular fragment transfers in a highly selective fashion.

Recent advances have demonstrated that base-metal catalysts can be significantly enhanced by "metal−ligand" cooperative effects, where ligands actively complement the metal by accepting or releasing electrons, protons, and/or functional units,[5,6] thereby mimicking enzyme-like behavior. This includes the redox "non-innocence" phenomenon, whereby ligands mediate electron transfers independently from the metal,[7] thus enhancing the versatility of catalysts in precious-metal-free transformations across a wide variety of substrates, including CO_2.[8] Particularly interesting are the 2,6-bis(imino)pyridine (BIP) ligands,[9] whose ability to reversibly take up to four electrons can impart "nobility" to base metals such as Co or Fe.[10,11] These BIP ligands enable such base metal complexes to catalyze reactions typically reserved for precious metals like C−C couplings,[12] hydrogenations,[13] hydrosilylations[14] or hydroborations.[15]

Building on the initial work on the interaction of [(BIP)Fe] systems with AlR_3 reagents reported by Gambarotta,[16] and some of us,[17] which led to the discovery of unusual paramagnetic organoaluminum $[(BIP\cdot)AlR_2]$ species, we have now devised their rational synthesis and unveiled their uniqueness to undergo reversible redox processes. Despite the established reactivity and applications in catalysis of some main-group metal $[(BIP)MX_n]$ complexes,[8,18,19] including Berben's systems with "AlH",[20] "AlCl"[21] and "$AlCl_2$"[22] fragments, a straightforward approach to reversibly manipulate reduced "Al^{2+}"-like species has remained elusive. Herein, we present a simple method for reversible ligand-centered reduction of aluminum species without significant structural alterations. We report the synthesis of cationic organo-aluminum complexes $[(BIP)AlR_2]^+$, **1**$^+$, and their reversible single-electron reduction to well-defined and isolable paramagnetic $[(BIP\cdot)AlR_2]$, **2** (Scheme 1). Our study expands the understanding of BIP redox capabilities with main-group metals and showcases reversible redox organoaluminum pairs $[(BIP)AlR_2]^{+/0}$, illustrating their potential for redox-mediated reactivity.

Received: June 27, 2024
Revised: September 18, 2024
Accepted: September 24, 2024
Published: October 4, 2024

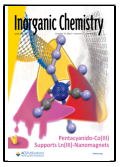

https://doi.org/10.1021/acs.inorgchem.4c02664
Inorg. Chem. 2024, 63, 19156−19166

Scheme 1. Syntheses of Cationic Aluminum Complexes $[(^{Ar'}BIP)AlR_2]^+$ 1$^+$ as $BAr^F{}_4^-$ or PF_6^- Salts and Reversible Redox Transformation to Paramagnetic Derivatives $[(^{Ar'}BIP^{\bullet})AlR_2]$ 2

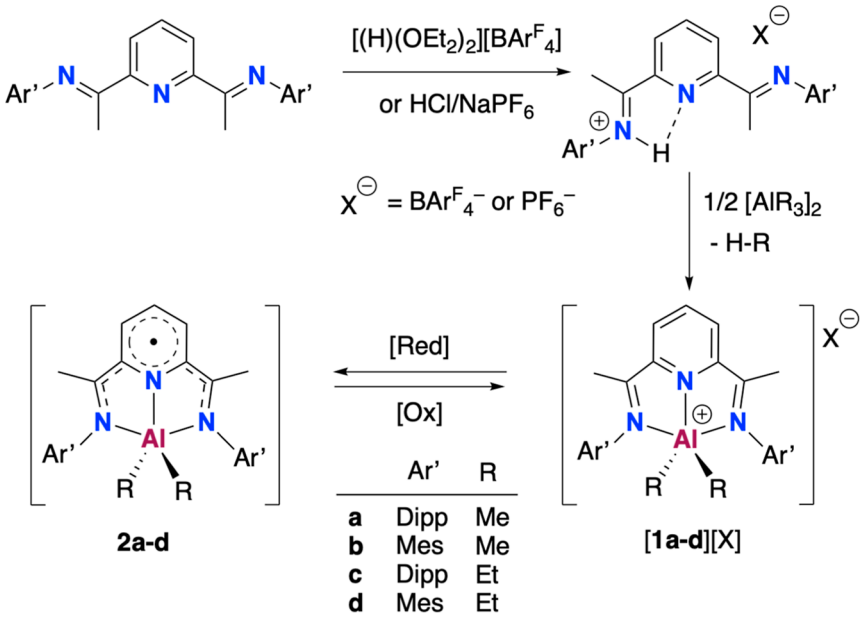

Dipp = 2,6-iPr$_2$C$_6$H$_3$, Mes = 2,4,6-Me$_3$C$_6$H$_2$, Ar^F = 3,5-(CF$_3$)$_2$C$_6$H$_3$

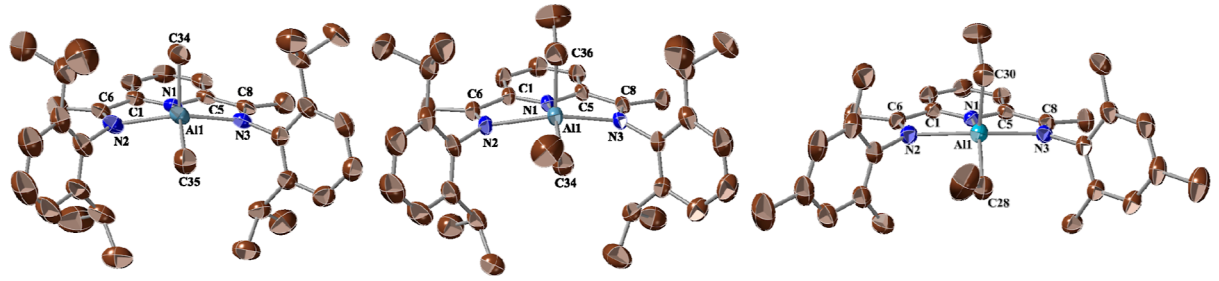

Figure 1. Crystal structures of [**1a**][$BAr^F{}_4$] (left), [**1c**][PF_6] (center) and [**1d**][$BAr^F{}_4$] (right), showing only the cationic organometallic units. All hydrogen atoms have been omitted for clarity. Selected bond lengths (Å) and angles (deg), approximately symmetrical bonds are given as averages: **1a**$^+$: Al1−N1, 2.011(4); Al−N(im), 2.152(3); C═N, 1.283(4); NC−C(Py), 1.492(4); N1−C, 1.339(4); Al1−C34, 1.959(5); Al1−C35, 1.945(5); N2−Al1−N(3), 144.32(15); N2−Al1−C35, 142.5(2). **1c**$^+$: Al1−N1, 1.997(3), Al1−N(im), 2.169(2); Al−C, 1.970(3); C═N, 1.281(3); NC−C(Py), 1.483(3); N1−C, 1.342(3); N2−Al1−N3, 144.51(12); N1−Al1−C, 114.8(2)-1**d**$^+$: Al1−N1, 2.019(2); Al−N(im), 2.177(1); Al−C, 1.972(2); C═N, 1.283(2); 1.484(2); N1−C, 1.344(2); N2−Al1−N3, 148.23(8); N1−Al1−C, 137.18(12).

RESULTS AND DISCUSSION

We synthesized the conjugated acids for the BIP ligands, $[^{Ar'}BIP(H)][BAr^F{}_4]$ (Scheme 1), which previously proved to be ideal precursors for accessing cationic alkyl metal complexes such as $[(^{Ar'}BIP)MnR][BAr^F{}_4]$[23] or $[(^{Ar'}BIP)ZnR][BAr^F{}_4]$.[24] Reacting equimolar amounts of these pro-ligand salts with alkyl reagents $AlMe_3$ or $AlEt_3$ led to the formation of the $BAr^F{}_4^-$ salts of the organoaluminum cations $[(^{Ar'}BIP)AlR_2]^+$ as orange-yellow crystalline solids in excellent yields of 90−95%. This selectivity was confirmed by NMR spectroscopy, which showed a single Al−R cleavage in each case. Additionally, we synthesized the PF_6^- salts of selected examples obtaining [**1a**][PF_6] and [**1c**][PF_6], in 91% and 87% yields, respectively. A related analog, $[(^{Dipp}BIP)AlEt_2][Al(OC_4F_9)_4]$, similar to [**1c**][$BAr^F{}_4$], was recently prepared by transmetalation from a low valent "$[(^{Dipp}BIP)Ga]^+$" precursor;[18] however, only a few crystals of this compound could be isolated, contrasting with the straightforward robustness of our method.

These cationic complexes were fully characterized, including by NMR spectroscopy (see Supporting Information for full details). Their ^{1}H NMR spectra show distinct, sharp signals for the BIP ligand with a characteristic resonance in the range δ 2.45−2.62 for the Me−C═N group. Additionally, these spectra display a single set of resonances for the Al-bound alkyl groups at $\delta \approx -0.91$ for $AlMe_2$ and $\delta \approx -0.05$ CH_2 and 0.12 CH_3 for $AlEt_2$, indicating chemical equivalency of both Me and Et groups.

The crystal structures of [**1a**][$BAr^F{}_4$], [**1c**][PF_6], and [**1d**][$BAr^F{}_4$] (Figure 1) reveal pentacoordinate Al centers, robustly coordinated by the BIP ligands in a slightly distorted square pyramidal configuration. The three N donor atoms from the tripodal BIP ligand and one C-alkyl atom form the base of the pyramid, while the second alkyl group occupies the apex. The Al atom is displaced by ca. 0.6 Å above the mean coordination plane formed by the BIP ligand, approaching the geometric center of the pyramid. The intraligand C═N, (Py)C−C(N) and αC−N(Py) bond lengths (ca. 1.28, 1.48 and 1.36 Å, respectively) are similar to those observed in

https://doi.org/10.1021/acs.inorgchem.4c02664
Inorg. Chem. 2024, 63, 19156−19166

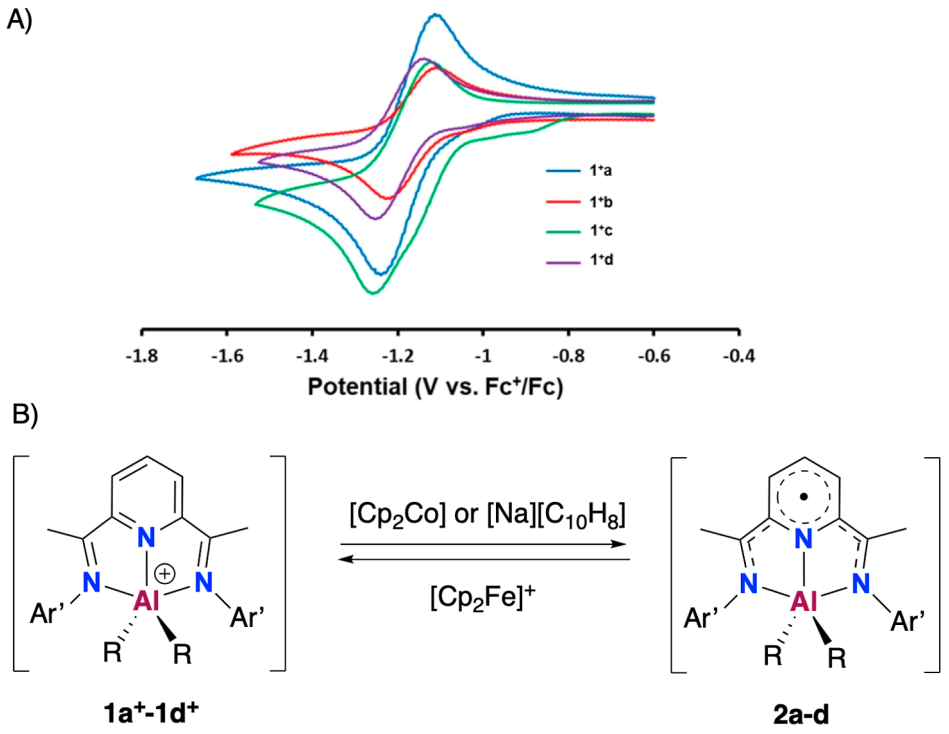

Figure 2. (A) CV traces for cationic complexes $\mathbf{1}^+$ (as $BAr^F{}_4{}^-$ salts) showing a single reduction event ($E^{o\prime}$ vs $Fc^{+/0}$, dichloromethane, 100 mV·s^{-1}, [TBA][PF_6]). (B) Reversible redox reactions involving the paramagnetic electroneutral derivatives [($^{Ar\prime}$BIP·)AlR_2] **2**.

unperturbed BIP ligands.[9c,25] The Al−N(Py) bond lengths are notably short (ca. 2.00 Å) compared to the relatively longer Al−N(imine) bonds (ca. 2.17 Å), presumably due to the steric hindrance of the bulky Ar groups. Although the solid-state structures of the cationic units $\mathbf{1}^+$ exhibit two distinct alkyl groups, this distinction is not observed in the solution NMR spectra, suggesting positional exchange between the apical and basal alkyl groups. This dynamic behavior evinces an intramolecular swinging motion with a low energy barrier, similar to the positional exchange processes observed in solution for analogous dialkyl complexes [(BIP)FeR_2][26] and [(BIP)ZnR_2].[27]

The derivatives [**1**][$BAr^F{}_4$] demonstrate remarkable stability, despite the typical high reactivity and hydrolytic sensitivity associated with organoaluminum compounds. They do not react with weak protic reagents such as common alcohols or traces of water, likely due to the reduced Lewis acidity of the coordinatively crowded Al centers. Solutions of complexes [**1**][$BAr^F{}_4$] in dichloromethane remained stable for days under a normal air atmosphere as long as these were kept in closed NMR tubes. No degradation was detected by NMR spectroscopy for over 2 days. Encouraged by their chemical stability in solution, we further explored their redox properties using cyclic voltammetry (CV), as illustrated in Figure 2A. Each [($^{Ar\prime}$BIP)-AlR_2][$BAr^F{}_4$] complex, [**1**][$BAr^F{}_4$], undergoes a single reversible reduction event within diffusion-controlled processes (Figures S21, S24, S27 and S30). The redox potentials exhibit slight variations depending on the Ar' substituents on the BIP ligands (Dipp: $\mathbf{1a}^+$ and $\mathbf{1c}^+$ with $E^{o\prime}$ = −1.17 V; Mes $\mathbf{1b}^+$ and $\mathbf{1d}^+$ with $E^{o\prime}$ = −1.19 V). In addition, the effect of the alkyl groups, "$AlMe_2$" or "$AlEt_2$", on their redox potentials is negligible, suggesting overall that the redox process is predominantly ligand-centered, involving the conjugated pyridine and imino moieties.

Interestingly, the presence of the AlR_2 unit appears to significantly stabilize the reduced forms, contributing to the reversibility of the redox process. In contrast, the CV study of the protonated salt of the ligand, [^{Dipp}BIP(H)][$BAr^F{}_4$] shows an irreversible reduction at a somewhat more positive potential ($E_P \approx -1.07$ V, Figure S31), highlighting the lower chemical stability of the resulting free radical [^{Dipp}BIP(H)·]. Additionally, when conducted in THF, the irreversible reduction of the free ^{Dipp}BIP ligand occurs at $E_p \approx -2.55$ V. The significant cathodic shift of the latter CV trace compared to [^{Dipp}BIP-(H)]$^+$ and the similar cationic species $\mathbf{1}^+$ is attributed to the absence of electrostatic compensation provided by the positive charge.

The reversibility and moderate reduction potentials of around −1.2 V for the cationic species $\mathbf{1a}^+$−$\mathbf{1d}^+$ suggested that a mild single-electron reductant such as cobaltocene, $CoCp_2$, could effectively reduce cations $\mathbf{1}^+$ ($[Cp_2Co]^{+/0}$, $E^{o\prime}$ = −1.33 V vs $Fc^{+/0}$ in dichloromethane).[28] In situ monitoring of the reaction of complexes [**1**][$BAr^F{}_4$] with one equivalent of Cp_2Co by ^{1}H NMR spectroscopy, in either CD_2Cl_2 or Tol-d_8, revealed complete disappearance of the resonances of $\mathbf{1a}^+$-$\mathbf{1d}^+$ within 20 min (see Supporting Information for further details). The resulting dark red-purple solutions exhibited only signals attributed to [Cp_2Co][$BAr^F{}_4$], suggesting the formation of paramagnetic aluminum species. Subsequently, adding one equivalent of ferrocenium hexafluorophosphate [Fc][PF_6] as an oxidant to these mixtures immediately restored the ^{1}H NMR signals of the diamagnetic cations $\mathbf{1}^+$. The restored spectra appeared somewhat broad and displayed slightly shifted resonances for the species $\mathbf{1}^+$, more pronounced for the $\mathbf{1c}^+$/**2c** redox pair (Figures S15−S18), likely due to minor variations in the system, such as ion pairing and exchange effects involving $[BAr^F{}_4]^-$ and $[PF_6]^-$ counterions, or the presence of residual paramagnetic species. These in situ reversible redox reactions are essentially quantitative as

https://doi.org/10.1021/acs.inorgchem.4c02664
Inorg. Chem. 2024, 63, 19156−19166

concluded from comparing the signal intensities with the residual solvent peaks. This encouraged us to isolate the corresponding paramagnetic organoaluminum species for detailed structural analyses.

Scaling up these NMR-monitored reductions with $[Cp_2Co]$ enabled us to isolate and fully characterize the reduced species, namely $[(^{Ar'}BIP^{\cdot})AlR_2]$ **2a**–**2d** (Figure 2A). Specifically, **2a** and **2c** were prepared in dichloromethane where the byproduct $[Cp_2Co][BAr^F{}_4]$ crystallized upon cooling to −36 °C, as confirmed by X-ray diffraction (see Supporting Information for full details). The $BAr^F{}_4^-$ salt of cobalticinium was removed by filtration, and precipitation with *n*-hexane allowed the isolation of **2a** and **2c**. Similarly, **2b** and **2d**, more soluble in aromatic solvents, were prepared in toluene, and the insoluble cobalticinium salt was filtered out, facilitating the isolation of **2b** and **2d**. Although complexes **2** were isolated as analytically pure red-purple solids in good to excellent yields (59–71%), this was challenging due to the high solubility of the $[Cp_2Co][BAr^F{}_4]$ salt. To overcome this, we replaced the cobaltocene reductant with the readily available reductant sodium naphthalene $[Na][C_{10}H_8]$ and replaced the $[BAr^F{}_4]^-$ anion with $[PF_6]^-$ to reduce the solubility issues and simplify product isolation. The reduction of $[\mathbf{1c}][PF_6]$ with freshly titrated $[Na][C_{10}H_8]$ in THF produced **2c** along with volatile naphthalene. The insolubility of $NaPF_6$ in *n*-hexane facilitated the isolation of **2c** in almost quantitative yield (88%, Figure 2B). In contrast, although using $[Cp_2Co][BF_4]$ as the reductant led to the formation of red-purple solutions, complex reaction mixtures were obtained, likely due to the incompatibility of the $[BF_4]^-$ anion with the reduced species **2**, leading to decomposition.

We successfully grew crystals of the new reduced species **2b** by cooling a saturated solution in toluene at −36 °C, which yielded crystals suitable for X-ray diffraction analysis (Figure 3). The key structural metrics of **2b** are consistent with those

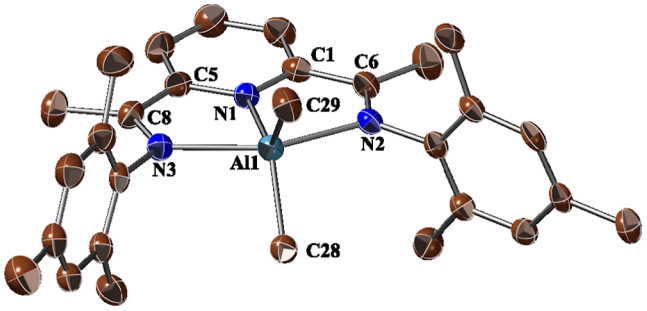

Figure 3. Crystal structure of **2b**. All hydrogen atoms have been omitted for clarity Thermal ellipsoids plot at 50% probability. Selected bond lengths (Å) and angles (deg): Al1–N1, 1.927(3); Al1–N2, 2.166(3); Al1–N3, 2.148(3); C6–N2, 1.304(5); C8–N3, 1.308(4); C1–C6, 1.439(6); C5–C8, 1.446(6); C1–N1, 1.381(5); C5–N1, 1.373(4); N1–Al–C29, 123.25(13); N2–Al1–N3, 153.21(10); C28–Al1–C29, 113.79(15).

previously reported for the analogs **2a**[16] and **2c**,[17] except for the variations in the aromatic substituents on the BIP ligands. The reduction from $\mathbf{1}^+$ to **2** is characterized by significant changes in bond lengths within the BIP ligand. For instance, considering averages for the three structures reported for each type of complex,[29] the imino C=N bond and α–C–N lengthen from 1.283(6) and 1.342(6) Å, respectively, in $\mathbf{1}^+$ to 1.313(6) and 1.373(7) Å, respectively, in **2** while the corresponding C(Py)–C(N) bonds at the pyridine ring shorten from 1.486(6) in $\mathbf{1}^+$ to 1.439(7) Å in **2**. These changes are consistent with the effects expected for a single-electron reduction of the BIP ligand.[9c,30]

Notably, the central Al–N(Py) bond in complexes **2**, averaging ca. 1.92 Å, is substantially shorter than in their oxidized counterparts $\mathbf{1}^+$ (average ca. 2.01 Å). However, the Al–N(imine) bond lengths remain similar between the oxidized and reduced complexes, averaging ca. 2.17 Å in both $\mathbf{1}^+$ and **2**. The geometry around the Al center also reflects changes due to the reduction of the systems. In particular, in the neutral methyl derivatives **2a** and **2b**, the Al atom is coplanar with the N3 donor set of the BIP ligand, aligning with a trigonal bipyramidal geometry as depicted in Figure 3. Conversely, in the slightly more hindered ethyl derivative **2c**,[17] the Al center deviates from the N3 plane, adopting a square-pyramidal geometry, similar to that observed in its cationic counterpart $\mathbf{1c}^+$.

The characterization of the paramagnetic species **2a**–**d** was completed with their IR and solution X-band electronic paramagnetic resonance (EPR) spectra. It is worth noting that their IR spectra lack the prominent band at ∼1600 cm^{-1}, characteristic of the C=N stretch of the BIP ligand. This is consistent with the reduced π-bond character of the BIP skeleton. The EPR spectra of **2b**–**d**, along with the previously characterized **2a**[16] (Figure 4) exhibit a signal at $g \approx 2.00$,

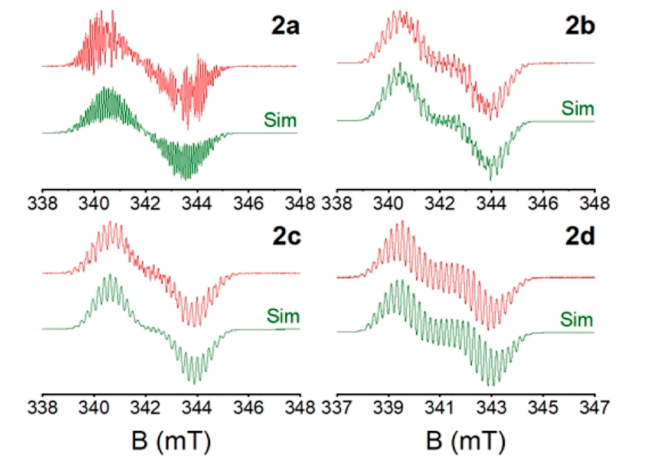

Figure 4. Experimental (top) and simulated (bottom) X-band EPR signals of **2a**–**d** in dichloromethane at 293 K.

indicative of a ligand-centered radical. In addition, the EPR spectra displayed a singular complex pattern for complexes **2** due to hyperfine couplings with the ^{27}Al ($I = 3/2$) and ^{15}N ($I = 1$) atoms from the pyridine and imine functions, along with several hydrogen ($I = 1/2$) nuclei. The values of these coupling constants, shown in Table 1, were determined by fitting the simulated signal shape to the experimental data. Our EPR results are in good agreement with those previously reported for **2a**,[16] underscoring their similar electronic structures. Our data confirm that the unpaired electron is more strongly coupled with the pyridine ^{15}N and the ^{27}Al nuclei, which suggests a significant contribution of the Al orbitals to the molecular SOMO, thereby modulating the radical-like nature and chemical stability of the paramagnetic species **2**. The hyperfine coupling constant to the ^1H atom at the pyridine's position 4 is remarkably large, which indicates a significant localization of the unpaired electron at this position. The

https://doi.org/10.1021/acs.inorgchem.4c02664
Inorg. Chem. 2024, 63, 19156–19166

Table 1. Main Isotropic g and Hyperfine Constants (A) for Complexes 2[a]

compound	2a	2b	2c	2d
ligand/R	^{Dipp}BIP/Me	^{Mes}BIP/Me	^{Dipp}BIP/Et	^{Mes}BIP/Et
g	2.0063	2.0049	2.0042	2.0063
A^{Al}	14.83	16.43	15.30	15.25
A^{Npy}	14.87	12.16	12.32	14.42
A^{Nim} (2)	4.99	2.99	5.18	4.94
A^{H4}	16.04	14.47	13.28	17.50
$A^{H3,3'}$(2)	2.57	5.13	2.16	5.02
A^{CH3} (6)	4.99	6.82	6.55	7.45
Fit RMSD	0.065	0.043	0.039	0.097

[a]10^{-3} M (toluene, 298 K). Number of equivalent nuclei shown in parentheses. For full listings of A values, see Supporting Information (Tables S1−S4).

couplings to other ^{1}H nuclei within the BIP ligands are smaller, and contributions from the Al-bonded methyl (Me) or ethyl (Et) groups are negligible (see Tables S1−S4). This pattern accounts for the observed high reactivity previously observed at the C4 position of the pyridine ring, although reactivity at the C3 position often competes.[31]

DFT calculations using the M06-L functional were performed to deepen our understanding of the redox behavior of the $[(^{Ar'}BIP)AlR_2]^{+/0}$ $\mathbf{1}^+/\mathbf{2}$ pairs in conjunction with the $[Cp_2Fe]^{+/0}$ and $[Cp_2Co]^{+/0}$ redox reagents.[32] The crystal geometries for complexes $\mathbf{1}^+$ and **2** were optimized at the M06-L/SV(P) level, using the CPCM solvation model in dichloromethane. A set of critical bond distances, including the C═N and C−C bonds in the BIP ligand, and the Al−N bonds, as well as the geometric τ_5 index,[33] calculated from the N(imine)−Al−N′(imine) and the largest N(Py)−Al−C angles, were used to assess the coordination geometries (see Supporting Information, Table S7). These calculations replicated the experimental crystal structures of the couples $\mathbf{1}^+/\mathbf{2}$, within an average deviation <1% between experimental and calculated bond lengths. The τ_5 value for the computed geometries showed consistent results with experimental data, indicating near-zero values for square-pyramidal (SQP) structures of $\mathbf{1}^+$ and **2b** species and approximately 0.5 for **2a** and **2b**, indicating trigonal-bipyramidal (TBP) geometries for the latter. The τ_5 index for an ideal trigonal-bipyramid is 1, but the nonlinearity along the main N2−Al−N3 axis decreases the geometry index to an intermediate value. For $\mathbf{1c}^+$ and **2d**, for which no experimental X-ray data is available, our calculations predicted SQP geometries ($\tau_5 \approx 0$). The vibrational M06-L/SV(P) calculations also predict a significant intensity loss of the ν(C═N) stretch band, and a shift to lower frequencies (ca. 100 cm^{-1}) on going from $\mathbf{1a}-\mathrm{d}^+$ to **2a**−d, explaining the difficulty of assigning this band in the IR spectra of the reduced species.

Single-point energy corrections at the M06-L/SVPD level provided accurate enough values of the free energy changes for the reversible redox reactions $\mathbf{1a}-\mathrm{d}^+ \leftrightarrow$ **2a**−d, thereby allowing precise computation of their ΔE^o potentials vs the ferrocene (Fc) or cobaltocene (*Cc*) redox couples. As a benchmark, the calculated potentials for the $[Fc]^{+/0}$ vs $[Cc]^{+/0}$ couples dichloromethane was −1.36 V, closely aligned with the experimental −1.33 V.[28] The calculated reduction potentials for the $\mathbf{1}^+/\mathbf{2}$ couples vs. were within the experimental range of −1.15 to −1.20 V vs $Fc^{+/0}$ (Table 2), and confirming their ability to oxidize *Cc*.

Table 2. Experimental and Calculated Reduction Potentials (V) vs (Fc^+/Fc)

redox pair	$\Delta E^{o'}$ Exptal[a]	ΔE^o Calcd[b]
Cc^+/Cc^{ref}	−1.33	−1.36
$\mathbf{1a}^+/\mathbf{2a}$	−1.17	−1.20
$\mathbf{1b}^+/\mathbf{2b}$	−1.19	−1.12
$\mathbf{1c}^+/\mathbf{2c}$	−1.17	−1.11
$\mathbf{1d}^+/\mathbf{2d}$	−1.19	−1.16

[a]vs Fc^+/Fc, in CH_2Cl_2, 293 K. [TBA][PF_6] background electrolyte. [b]M06-L,CPCM-CH_2Cl_2/SVPD//SV(P).

Additionally, we computed the EPR parameters for paramagnetic complexes **2**. While EPR parameters for **2a** were initially approximated using the BP86 or B3LYP functionals,[16] the *meta*-GGA functional BW6D95 paired with the EPR-II and def2-TZVP (for Al) basis sets yielded slightly more consistent results across complexes **2a**−**d**. A full description of the computational methodology and comparative results are collected in the Supporting Information (Tables S10−S13).

CONCLUSIONS

In this study, we have established a general methodology for synthesizing reduced aluminum paramagnetic species $[(BIP\cdot)AlR_2]$ through the chemical reduction of their isostructural cations $[(BIP)AlR_2]^+$ using mild one-electron redox reagents, like $[Cp_2Co]$. The organoaluminum precursors $[(BIP)AlR_2]^+$ were conveniently synthesized as stable $BAr^F{}_4^-$ or PF_6^- salts by the reaction of the conjugate acids of BIP ligands, with commercial aluminum reagents, $AlMe_3$ and $AlEt_3$. Furthermore, we demonstrated the reversibility of the redox process involving the $[(BIP)AlR_2]^{+/0}$ couples, both electrochemically via voltammetry and chemically with $[Cc]$ and $[Fc]^+$ reagents. The redox processes linking the diamagnetic $[(BIP)AlR_2]^+$ and paramagnetic $[(BIP\cdot)AlR_2]$ species were characterized in detail using a suite of spectroscopic, crystallographic, electrochemical, and computational methods to confirm their mild exchange potentials and redox reversibility. These findings significantly advance our understanding of BIP ligand redox capabilities with main-group metals, particularly with Earth-abundant aluminum, paving the way for future studies into their reactivity and potential applications in redox catalysis.

EXPERIMENTAL SECTION

Most compounds presented in this work are highly sensitive to oxygen and moisture. Therefore, inert atmosphere Schlenk techniques and a N_2-filled glovebox were routinely used in manipulations and procedures. All solvents (dichloromethane, toluene, *N*-hexane, tetrahydrofuran and diethyl ether) were rigorously degassed, dried, and distilled immediately prior to use. Instrumentation and procedures, NMR, IR and EPR spectra of new compounds, elemental analysis (EA), X-ray diffraction studies, electrochemistry and computational details are included in the Supporting Information.

Solutions of HCl (2 M in diethyl ether) and $NaPF_6$ were supplied by Thermo Scientific, stored in a glovebox and employed as received. Aluminum trialkyls ($AlMe_3$, pure and 2 M in toluene and $AlEt_3$ 1.0 M in hexane) were purchased from Sigma-Aldrich and used as received. The protonated tetraarylborate salts $[H^{DippBIP}][BAr^F{}_4]$ and $[H^{MesBIP}][BAr^F{}_4]$ where ^{Dipp}BIP is 2,6-[2,6-^{i}Pr$_2$C$_6$H$_3$N═C(Me)]$_2$-C$_5$H$_3$N, ^{Mes}BIP is 2,6-[2,4,6-Me$_3$C$_6$H$_2$N═C(Me)]$_2$-C$_5$H$_3$N, and $Ar^F{}_4$ is (3,5-(CF$_3$)$_2$C$_6$H$_3$) respectively, were prepared according to our own reported methodology.[23] Bis(cyclopentadienyl)cobalt (Cp_2Co, where Cp═C$_5$H$_5$) in powder form, purchased from Alfa Aesar was stored at −30 °C within a glovebox and used without further purification. Ferrocenium hexafluorophosphate ($[Cp_2Fe][PF_6]$ with Cp═C$_5$H$_5$,

https://doi.org/10.1021/acs.inorgchem.4c02664
Inorg. Chem. 2024, 63, 19156−19166

abbreviated as [Fc][PF_6]), sourced from Merck, was also stored in a glovebox and used as received.

Synthesis of [^{Dipp}BIPH][Cl]. A 2 M solution in Et_2O of HCl (206.0 μL, 0.412 mmol) was added dropwise to stirred suspension of ^{Dipp}BIP (198.1 mg, 0.412 mmol) in Et_2O (20 mL) at −30 °C. The resulting pale-yellow solution was stirred for 30 min at room temperature. Then, the solvent was evaporated under vacuum, isolating a pale-yellow solid residue that corresponded to [^{Dipp}BIPH]-[Cl] (204.4 mg; 96%). **^{1}H NMR** (C_6D_6, 25 °C, 400 MHz): δ 1.13 (d, $^3J_{HH}$ = 6.9 Hz, 12H, CH*Me*Me), 1.22 (d, $^3J_{HH}$ = 6.9 Hz, 12H, CHMe*Me*), 2.27 (s, 6H, *Me*(CN)), 2.91 (sept, $^3J_{HH}$ = 7.0 Hz, 4H, *CH*MeMe), 7.15 (m, 6H, CH_{N-Ar}), 7.43 (br s, 1H, 4-CH_{py}), 8.66 (d, $^3J_{HH}$ = 7.9 Hz, 2H, 3-CH_{py}). **^{13}C{^{1}H} NMR** (C_6D_6, 25 °C, 100 MHz): δ 17.57 (*Me*−CN), 23.02 (CHMe*Me*), 23.67 (CH*Me*Me), 28.96 (*C*HMeMe), 123.78 (3,5-CH_{Py}), 125.43 (*m*-CH_{N-Ar}), 136.91 (*o*-C_{N-Ar}), 137.76 (4-CH_{Py}), 144.46 (*i*-CH_{N-Ar}), 154.05 (2-CH_{Py}), 168.97 (Me−*C*N). *The signal attributed to p-*CH_{N-Ar} was not-observed. **EA for $C_{33}H_{44}ClN_3$** (found vs calculated, crystalline sample): C 76.42 (76.49), H 8.28 (8.56), N 8.29 (8.11).

Synthesis of [^{Dipp}BIPH][PF_6]. In a nitrogen-filled glovebox, 53.7 mg (0.320 mmol) of $NaPF_6$ are slowly added to a pale-yellow solution of [^{Dipp}BIPH][Cl] (150 mg, 0.290 mmol), dissolved in 20 mL of THF, cooled to −30 °C. The solution instantly changed to orange. After 1 h stirring at room temperature, the solvent and volatiles were removed at reduced pressure. The solid residue was extracted in dichloromethane, filtered and dried again. The NMR spectra of the isolated orange solid corresponded exclusively to compound [^{Dipp}BIPH][PF_6] (163.6 mg, 90%). **^{1}H NMR** (CD_2Cl_2, 25 °C, 400 MHz): δ 1.14 (d, $^3J_{HH}$ = 6.9 Hz, 12H, CH*Me*Me), 1.19 (d, $^3J_{HH}$ = 7.0 Hz, 12H, CHMe*Me*), 2.45 [s, 6H, *Me*(CN)], 2.70 (sept, $^3J_{HH}$ = 7.1 Hz 4H, *CH*MeMe), 7.25 (br s, 6H, CH_{N-Ar}) 8.46 (br s, 1H, 4-CH_{py}), 8.65 (br s, 2H, 3-CH_{py}). **^{19}F{^{1}H} NMR** (CD_2Cl_2, 25 °C, 376 MHz): δ −72.91 (d, J_{FP} = 718.0 Hz, [PF_6]$^-$). **^{31}P{^{1}H} NMR** (CD_2Cl_2, 25 °C, 162 MHz): δ −144.56 (sept, J_{PF} = 716.0 Hz, [PF_6]$^-$). **^{13}C{^{1}H} NMR** (CD_2Cl_2, 25 °C, 100 MHz): δ 17.39 (*Me*−CN), 22.87 (CHMe*Me*), 23.58 (CH*Me*Me), 29.07 (*C*HMeMe), 124.12 (3,5-CH_{Py}), 127.54 (*m*-CH_{N-Ar}), 128.91 (*p*-CH_{N-Ar}), 138.07 (*o*-C_{N-Ar}), 143.79 (4-CH_{Py}), *not observed* (*i*-CH_{N-Ar}), *not observed* (2-CH_{Py}), 168.50 (Me−*C*N). **EA for $C_{33}H_{44}PF_6N_3$** (found vs calculated, crystalline sample): C 63.12 (63.15), H 7.31 (7.07), N 6.83 (6.69).

Synthesis of [Al(Me)$_2$(^{Dipp}BIP)][PF_6] ([1a][PF_6]). A 5 mL CH_2Cl_2 cold (−25 °C) colorless solution of $AlMe_3$ (32 μL, 0.313 mmol) was slowly added to another orange CH_2Cl_2 solution (15 mL) of [^{Dipp}BIPH][PF_6] (178.5 mg; 0.285 mmol) at the same temperature, immediately changing to a yellow-brown. The mixture was stirred vigorously for 10 min, and then, the solvent and volatiles were removed under vacuum. The solid residue was washed with hexane (3 × 5 mL). Finally, the product was filtered and dried at reduced pressure, obtaining a yellow-brown powdery solid (177.2 mg, 91%) that corresponded to complex [**1a**][PF_6]. **^{1}H NMR** (CD_2Cl_2, 25 °C, 300 MHz): δ −0.92 (s, 6H, AlMe_2), 1.09 (d, $^3J_{HH}$ = 7.0 Hz, 12H, CH*Me*Me), 1.23 (d, $^3J_{HH}$ = 6.9 Hz, 12H, CHMe*Me*), 2.57(sept, $^3J_{HH}$ = 6.9 Hz, 4H, *CH*MeMe), 2.59 (s, 6H, *Me*(CN)), 7.30 (d, $^3J_{HH}$ = 7.3 Hz, 4H, *m*-CH_{N-Ar}), 7.38 (t, $^3J_{HH}$ = 7.4 Hz, 2H, *p*-CH_{N-Ar}), 8.68 (d, $^3J_{HH}$ = 7.9 Hz, 2H, 3-CH_{py}), 8.95 (t, $^3J_{HH}$ = 8.1 Hz, 1H, 4-CH_{py}). **^{19}F{^{1}H} NMR** (CD_2Cl_2, 25 °C, 376 MHz): δ −72.80 (d, J_{FP} = 718.0 Hz, [PF_6]$^-$). **^{31}P{^{1}H} NMR** (CD_2Cl_2, 25 °C, 162 MHz): δ −144.55 (sept, J_{PF} = 716.0 Hz, [PF_6]$^-$). **^{13}C{^{1}H} NMR** (CD_2Cl_2, 25 °C, 100 MHz): δ −7.93 (AlMe_2), 19.27 (*Me*−CN), 24.15 (CHMe*Me*), 25.15 (CH*Me*Me), 29.16 (*C*HMeMe), 125.14 (*m*-CH_{N-Ar}), 128.70 (3,5-CH_{Py}), 129.35 (*p*-CH_{N-Ar}), 139.35 (*o*-C_{N-Ar}), 140.25 (*i*-C_{N-Ar}), 147.73 (4-CH_{Py}), 148.07 (2-CH_{Py}), 171.10 (Me−*C*N). IR (KBr/Nujol, cm-1): ν 1600 (Intense, C=N stretch). **EA for $C_{35}H_{49}AlPF_6N_3$** (found vs calculated, crystalline sample): C 61.46 (61.48), H 7.48 (7.22), N 6.21 (6.15).

Synthesis of [Al(Me)$_2$(^{Dipp}BIP)][BAr^F_4] ([1a][BAr^F_4]). A dichloromethane (5 mL) solution of trimethyl aluminum ($AlMe_3$, 11.6 μL, 0.121 mmol) was added via pipette to another CH_2Cl_2 solution (15 mL) of [(^{Dipp}BIPH)][BAr^F_4] (142.5 mg; 0.101 mmol) both at −25 °C, observing an instantaneous change from orange to yellow-green. The reaction mixture was magnetically stirred for 16 h. Then, the solvent and volatiles were removed at vacuo, isolating a solid which upon washing with hexane (3 × 5 mL), filtration and drying allow obtaining a yellow-green powdery solid (131.6 mg, 93%) that corresponded with ([**1a**][BAr^F_4]). Recrystallization in a cold (−35 °C) CH_2Cl_2: hexane (5:1) solution produced yellow cubic crystals suitable for X-ray diffraction studies. **^{1}H NMR** (CD_2Cl_2, 25 °C, 400 MHz): δ −0.91 (s, 6H, AlMe_2), 1.08 (d, $^3J_{HH}$ = 6.9 Hz, 12H, CH*Me*Me), 1.22 (d, $^3J_{HH}$ = 6.9 Hz, 12H, CHMe*Me*), 2.51 (sept, $^3J_{HH}$ = 6.9 Hz, 4H, *CH*MeMe), 2.55 (s, 6H, *Me*(CN)), 7.31 (d, $^3J_{HH}$ = 7.3 Hz, 4H, *m*-CH_{N-Ar}), 7.40 (t, $^3J_{HH}$ = 7.4 Hz, 2H, *p*-CH_{N-Ar}), 7.55 (s, 4H, *p*-CH_{Ar} BAr^F_4), 7.72 (br s, 8H, *o*-CH_{Ar} BAr^F_4), 8.45 (d, $^3J_{HH}$ = 7.9 Hz, 2H, 3-CH_{py}), 8.68 (d, $^3J_{HH}$ = 8.0 Hz, 1H, 4-CH_{py}). **^{19}F{^{1}H} NMR** (CD_2Cl_2, 25 °C, 376 MHz): δ −62.87 (s, BAr^F_4). **^{11}B{^{1}H} NMR** (CD_2Cl_2, 25 °C, 128 MHz): δ −6.61 (s, BAr^F_4). **^{13}C{^{1}H} NMR** (CD_2Cl_2, 25 °C, 100 MHz): δ −7.80 (AlMe_2), 19.22 (*Me*−CN), 24.09 (CHMe*Me*), 25.01 (CH*Me*Me), 29.33 (*C*HMeMe), 117.90 (*p*-CH_{Ar} BAr^F_4), 123.64 (*m*-CH_{N-Ar}), 125.33 (CF_3 BAr^F_4), 126.35 (3,5-CH_{Py}), 128.35 (*p*-CH_{N-Ar}), 129.23 (q, $^2J_{CF}$ = 33 Hz, *C*-CF_3 BAr^F_4), 135.21 (*o*-CH_{Ar} BAr^F_4), 138.95 (*o*-C_{N-Ar}), 139.81 (*i*-C_{N-Ar}), 147.16 (4-CH_{Py}), 147.94 (2-CH_{Py}), 162.11 (q, $^1J_{CB}$ = 50 Hz, *i*-C_{Ar} BAr^F_4), 170.12 (Me−*C*N). **EA for $C_{67}H_{61}AlBF_{24}N_3$** (found vs calculated, crystalline sample): C 57.42 (57.40), H 4.51 (4.39), N 2.85 (3.00).

Synthesis of (^{Dipp}BIP·)AlMe_2 (2a). A J. Young's ampule was loaded with 200 mg (0.142 mmol) of [**1a**][BAr^F_4] and 27 mg (0.142 mmol) of Cp_2Co. The solids were combined with 3 mL of dry dichloromethane to form a dark purple suspension. This mixture was stirred vigorously at room temperature and progress was monitored via ^{1}H NMR analysis of aliquots. After 4 h, the resonances attributed to [**1a**][BAr^F_4] disappeared. The mixture was then filtered through a cannula into a Schlenk tube and cooled to −36 °C. After 16 h, single crystals of [Cp_2Co][BAr^F_4] suitable for X-ray crystallography were harvested. This crystalline material was filtered to give a dark purple solution. The resulting dark purple solution was concentrated to 1 mL, and the addition of 20 mL of anhydrous *n*-hexane precipitated a purple solid. This product was isolated by cannula filtration and dried under high vacuum (<10^{-2} mbar), affording (^{Dipp}BIP·)AlMe_2 (**2a**) as a dark purple solid (Yield: 46 mg, 0.084 mmol, 59%.), according to its EA and its EPR spectrum, which can be checked in the Supporting Information. Single crystals suitable for X-ray diffraction analysis were obtained by cooling a toluene solution of **2a** at −36 °C for 24 h. The X-ray crystal structure of (^{Dipp}BIP·)AlMe_2 (**2a**) obtained in this study is consistent with the structure earlier reported by Gambarotta.[2] This confirmation reinforces the reproducibility of the crystalline structure under the described synthesis conditions.

Note on ^{1}H NMR Data: *The absence of ^{1}H NMR resonances for (^{Dipp}BIP·)AlMe_2 (**2a**) is attributable to the paramagnetic nature of the compound.* **EA for $C_{35}H_{49}AlN_3$** (found vs calculated, crystalline sample): C 78.08 (78.03), H 9.30 (9.17), N 7.99 (7.80). **IR (KBr/Nujol, cm^{-1})**: ν 1644, 1607, 1587 (medium intensity, C=C Py and C=N imine). *The bands observed at 1644 cm^{-1} for the C=C stretch is characteristic of the dearomatized pyridine ring.*

Synthesis of [Al(Me)$_2$(^{Mes}BIP)][BAr^F_4] ([1b][BAr^F_4]). To 148 mg (0.118 mmol) of [(^{Mes}BIPH)][BAr^F_4] in 15 mL of CH_2Cl_2 at −25 °C was added 13.5 μL (0.142 mmol) of $AlMe_3$ in 5 mL of CH_2Cl_2 via syringe. Then, the same experimental protocol used for the preparation of [**1a**][BAr^F_4] was applied to the synthesis of [**1b**][BAr^F_4], isolating a brown solid (150.8 mg, 95%) which according to the NMR spectra corresponded to the expected compound [**1b**][BAr^F_4]. Recrystallization attempts did not afford suitable crystals for X-ray diffraction studies. **^{1}H NMR** (CD_2Cl_2, 25 °C, 400 MHz): δ −0.91 (s, 6H, AlMe_2), 2.01 (s, 12H, *o*-Me_{N-Ar}), 2.36 (s, 6H, *p*-Me_{N-Ar}), 2.47 (s, 6H, *Me*−CN), 7.01 (s, 4H, *m*-CH_{N-Ar}), 7.59 (s, 4H, *p*-CH_{Ar} BAr^F_4), 7.76, (br s, 8H, *o*-CH_{Ar} BAr^F_4), 8.48 (d, $^3J_{HH}$ = 8.0 Hz, 2H, 3-CH_{py}), 8.73 (d, $^3J_{HH}$ = 7.8 Hz, 1H, 4-CH_{py}). **^{19}F{^{1}H} NMR** (CD_2Cl_2, 25 °C, 376 MHz): δ −62.82 (s, BAr^F_4). **^{11}B{^{1}H} NMR** (CD_2Cl_2, 25 °C, 128 MHz): δ −6.61 (s, BAr^F_4). **^{13}C{^{1}H} NMR** (CD_2Cl_2, 25 °C, 100 MHz): δ −9.67 (AlMe_2), 14.29,

https://doi.org/10.1021/acs.inorgchem.4c02664
Inorg. Chem. 2024, 63, 19156−19166

17.19 (*Me*−CN), 18.37 (*o*-Me_{N-Ar}), 20.87 (*p*-Me_{N-Ar}), 117.90 (*p*-CH_{Ar} BAr^F_4), 123.64 (CF_3 BAr^F_4), 128.10 (3,5-CH_{Py}), 128.53 (*p*-C_{N-Ar}), 129.28 (q, $^2J_{CF}$ = 33 Hz, *C*-CF_3 BAr^F_4), 130.36 (*m*-CH_{N-Ar}), 135.25 (*o*-CH_{Ar} BAr^F_4), 137.87 (*o*-C_{N-Ar}), 138.95 (*i*-C_{N-Ar}), 147.50 (4-CH_{Py}), 149.14 (2-CH_{Py}), 162.10 (q, $^1J_{CB}$ = 50 Hz, *i*-C_{Ar} BAr^F_4), 169.22 (Me−CN). **EA for** $C_{61}H_{49}AlBF_{24}N_3$ (found vs calculated, bulk sample): C 55.65 (55.60), H 4.04 (3.75), N 3.22 (3.19).

Synthesis of (^{Mes}BIP·)AlMe$_2$ (2b). A J. Young's ampule was charged with 233 mg (0.177 mmol) of [**1b**][BAr^F_4] and 33 mg (0.177 mmol) of Cp_2Co. The solids were combined with 3 mL of anhydrous toluene, forming a dark red suspension. This mixture was stirred vigorously at room temperature and progress was monitored via ^{1}H NMR analysis of aliquots. After 4 h, the resonances attributed to [**1b**][BAr^F_4]disappeared. After this time, the reaction mixture was filtered into a Schlenk tube via cannula to remove the salt [Cp_2Co][BAr^F_4] precipitated. Then, dry *n*-hexane was added dropwise to the resulting solution to point of incipient crystallization. The Schlenk tube was then stored at −36 °C overnight. The resultant solid was isolated via cannula filtration, dried under high vacuum (<10^{-2} mbar), yielding (^{Mes}BIP·)AlMe$_2$ (**2b**) as a dark red solid. Yield: 57 mg, 0.125 mmol, 71%. Suitable plate-shaped single crystals of **2b** for X-ray diffraction analysis were obtained by layering a toluene solution (1 mL) of the compound with *n*-hexane (2 mL) and progressively cooling down the mixture to 0 °C for 4 h and then from 0 °C to −36 °C overnight. **Note on ^{1}H NMR data:** *The absence of ^{1}H NMR resonances for (^{Mes}BIP·)AlMe$_2$ (**2b**) is attributable to the paramagnetic nature of the compound.* **EA for** $C_{29}H_{37}AlN_3$ (found vs calculated, bulk sample): C 76.63 (76.62), H 8.30 (8.20), N 9.01 (9.24). **IR (KBr/Nujol, cm^{-1}):** ν 1640, 1609, 1557 (medium to weak intensity, C═C Py and C═N imine). *The band observed at 1640 cm^{-1} for the C═C stretch is characteristic of the dearomatized pyridine ring.* The **EPR** of **2b** spectrum is available in the Supporting Information.

Synthesis of [Al(Et)$_2$(^{Dipp}BIP)][BAr^F_4] [1c][BAr^F_4]. The synthesis of [**1c**][BAr^F_4] was carried out following a similar experimental protocol than that applied for the preparation of [**1a**][BAr^F_4]. To 120.0 mg (0.089 mmol) of [(^{Dipp}BIP)]$^+$[BAr^F_4]$^-$ in 15 mL of CH_2Cl_2 at −25 °C was added 106.8 μL (0.107 mmol) of $AlEt_3$ 106.8 μL (0.107 mmol, 1 M in *n*-hexane). An orange powdery solid (114.5 mg, 90%) was isolated which according to the NMR spectra corresponded solely to compound [**1c**][BAr^F_4]. **^{1}H NMR** (CD_2Cl_2, 25 °C, 300 MHz): δ −0.05 (q, $^3J_{HH}$ = 8.0 Hz, 4H, Al(CH_2CH_3)$_2$), 0.11 (t, $^3J_{HH}$ = 7.0 Hz 6H, Al(CH_2CH_3)$_2$), 1.09 (d, $^3J_{HH}$ = 6.9 Hz, 12H, CH*Me*Me), 1.26 (d, $^3J_{HH}$ = 6.8 Hz, 12H, CHMe*Me*), 2.49 (sept, $^3J_{HH}$ = 6.5 Hz, 4H, *CH*MeMe), 2.57 (s, 6H, *Me*(CN)), 7.32 (d, $^3J_{HH}$ = 7.7 Hz, 4H, *m*-CH_{N-Ar}), 7.42 (t, $^3J_{HH}$ = 7.7 Hz, 2H, *p*-CH_{N-Ar}), 7.56 (s, 4H, *p*-CH_{Ar} BAr^F_4), 7.73 (br s, 8H, *o*-CH_{Ar} BAr^F_4), 8.47 (d, $^3J_{HH}$ = 8.0 Hz, 2H, 3-CH_{py}), 8.65 (d, $^3J_{HH}$ = 8.0 Hz, 1H, 4-CH_{py}). **^{19}F{^{1}H} NMR** (CD_2Cl_2, 25 °C, 376 MHz): δ −62.82 (s, BAr^F_4). **^{11}B{^{1}H} NMR** (CD_2Cl_2, 25 °C, 128 MHz): δ −6.59 (s, BAr^F_4). **^{13}C{^{1}H} NMR** (CD_2Cl_2, 25 °C, 100 MHz): δ −1.29 (Al(CH_2CH_3)$_2$), 8.10 (Al(CH_2CH_3)$_2$), 19.20 (*Me*−CN), 23.92 (CHMe*Me*), 25.11 (CH*Me*Me), 29.31 (CHMeMe), 117.91 (*p*-CH_{Ar} BAr^F_4), 123.66 (*m*-CH_{N-Ar}), 125.34 (CF_3 BAr^F_4), 126.36 (3,5-CH_{Py}), 127.99 (*p*-CH_{N-Ar}), 129.30 (q, $^2J_{CF}$ = 30 Hz, *C*-CF_3 BAr^F_4), 135.23 (*o*-CH_{Ar} BAr^F_4), 139.55 (*o*-C_{N-Ar}), 139.85 (*i*-C_{N-Ar}), 146.77 (4-CH_{Py}), 147.72 (2-CH_{Py}), 162.21 (q, $^1J_{CB}$ = 50 Hz, *i*-C_{Ar} BAr^F_4), 170.41 (Me−CN). **EA for** $C_{69}H_{65}AlBF_{24}N_3$ (found vs calculated, bulk sample): C 57.88 (57.95), H 4.21(4.58), N 3.16(2.94).

Synthesis of [Al(Et)$_2$(^{Dipp}BIP)][PF_6] ([1c][PF_6]). An orange solution of [^{Dipp}BIPH][PF_6] (130.2 mg; 0.208 mmol) in 15 mL of CH_2Cl_2 was reacted with another of $AlEt_3$ 1 M in hexane (208 μL, 0.208 mmol) at −30 °C. The resultant solution immediately changed to a yellow-brown color and this was kept under magnetic stirring for 10 min. The solvent and volatiles were then removed under vacuum, isolating a crude orange solid. This residue was washed with hexane (3 × 5 mL), filtered and evaporated to dryness, producing a yellow-brown powdery solid corresponding with [**1c**][PF_6] (128.3 mg, 87%). Then, this was dissolved in 1 mL of CH_2Cl_2 and subsequently 0.1 mL of hexane. The resulting solution was stored at −30 °C and after 72 h, a yellow cubic microcrystalline solid appeared that was suitable for X-ray diffraction studies. **^{1}H NMR** (CD_2Cl_2, 25 °C, 300 MHz): δ −0.06 (q, $^3J_{HH}$ = 8.3 Hz, 4H, Al(CH_2CH_3)$_2$), 0.13 (t, $^3J_{HH}$ = 7.9 Hz 6H, Al(CH_2CH_3)$_2$), 1.12 (d, $^3J_{HH}$ = 6.9 Hz, 12H, CH*Me*Me), 1.28 (d, $^3J_{HH}$ = 6.9 Hz, 12H, CHMe*Me*), 2.55 (sept, $^3J_{HH}$ = 6.5 Hz, 4H, *CH*MeMe), 2.62 (s, 6H, *Me*(CN)), 7.32 (d, $^3J_{HH}$ = 7.7 Hz, 4H, *m*-CH_{N-Ar}), 7.41 (t, $^3J_{HH}$ = 7.7 Hz, 2H, *p*-CH_{N-Ar}), 8.69 (d, $^3J_{HH}$ = 8.0 Hz, 2H, 3-CH_{py}), 8.92 (t, $^3J_{HH}$ = 8.0 Hz, 1H, 4-CH_{py}). **^{19}F{^{1}H} NMR** (CD_2Cl_2, 25 °C, 376 MHz): δ −72.96 (d, J_{FP} = 710.0 Hz, [PF_6]$^-$). **^{31}P{^{1}H} NMR** (CD_2Cl_2, 25 °C, 162 MHz): δ −144.54 (sept, J_{PF} = 712.0 Hz, [PF_6]$^-$). **^{13}C{^{1}H} NMR** (CD_2Cl_2, 25 °C, 100 MHz): δ −1.40 (Al(CH_2CH_3)$_2$), 8.14 (Al(CH_2CH_3)$_2$), 19.19 (*Me*−CN), 23.91 (CHMe*Me*), 25.20 (CH*Me*Me), 29.12 (CHMeMe), 125.10 (*m*-CH_{N-Ar}), 128.73 (3,5-CH_{Py}), 128.89 (*p*-CH_{N-Ar}),, 139.87 (*o*-C_{N-Ar}), 140.18 (*i*-C_{N-Ar}), 147.47 (4-CH_{Py}), 147.67 (2-CH_{Py}), 171.33 (Me−*C*N). **EA for** $C_{37}H_{53}AlPF_6N_3$ (found vs calculated, bulk sample): C 62.44 (62.43), H 7.50 (7.51), N 5.92 (5.90). **IR (KBr/Nujol, cm^{-1}):** ν 1597 (C═N, BIP).

Synthesis of (^{Dipp}BIP·)AlEt$_2$ (2c). *Route A.* A J. Young's ampule was loaded with 397 mg (0.277 mmol) of [**1c**][BAr^F_4] and 54 mg (0.282 mmol) of Cp_2Co. The solids were combined with 3 mL of anhydrous dichloromethane, giving a dark red suspension. This mixture was stirred vigorously at room temperature and progress was monitored via ^{1}H NMR analysis of aliquots. After 4 h, the resonances attributed to [**1c**][BAr^F_4] disappeared. Subsequent cooling of the mixture to −36 °C initiated the precipitation of [Cp_2Co][BAr^F_4]. After 2 h at this temperature, the cold mixture was filtered and the filtrate was dried under vacuum (<10^{-2} mbar) to yield (^{Dipp}BIP·)-AlEt$_2$ (**2c**) as a dark golden/brown solid. Yield: 81 mg, 0.142 mmol, 51%. Crystallization was attempted with several solvent mixtures but not achieved. **Note on ^{1}H NMR data:** *The absence of ^{1}H NMR resonances for (^{Dipp}BIP·)AlEt$_2$ (**2c**) is attributable to the paramagnetic nature of the compound.* **IR (KBr/Nujol, cm^{-1}):** ν 1643, 1607, 1584 (medium to weak intensity, C═C Py and C═N imine). *The band observed at 1643 cm^{-1} for the C═C stretch is characteristic of the dearomatized pyridine ring.*

Synthesis of 2c. *Route B.* Compound [**1c**][PF_6] (82.2 mg; 0.115 mmol) was dissolved in 10 mL of THF and cooled to −30 °C. Then, 131 μL of a solution of sodium-naphthalene (0.88 M in THF, 0.115 mmol) was added at the same temperature. The orange solution turned brown immediately, being stirred for 30 min at room temperature. Then, the solvent and volatiles were dried under vacuum. The solid residue was then extracted in hexane (3 × 5 mL), filtered and brought to dryness, yielding 57.6 mg (88%) of a brown solid corresponding to complex **2c**. Although the synthesis and full characterization of **2c** has already been reported by us,[17] this route provide pure samples as the corresponding **EA for** $C_{37}H_{53}AlN_3$ (found vs calculated): C 78.48 (78.40), H 9.66 (9.48), N 7.30 (7.41) and **EPR spectrum** (see Supporting Information) confirmed.

Synthesis of [Al(Et)$_2$(^{Mes}BIP)][BAr^F_4] ([1d][BAr^F_4]). The same experimental protocol employed for the preparation of ([**1a**][BAr^F_4]) was used for the synthesis of ([**1d**][BAr^F_4]). To 252.0 mg (0.200 mmol) of [(^{Mes}BIPH)][BAr^F_4], 239.8 μL (0.240 mmol) of $AlEt_3$ (1 M in hexane) was added via pipet, both at approximately −25 °C. An orange solid that according to the NMR spectra corresponded to [**1d**][BAr^F_4]. was isolated (250.2 mg, 93%). Then, this was dissolved in a CH_2Cl_2/hexane (4:1) mixture and stored at −35 °C. An orange crystalline solid suitable for X-ray diffraction studies was obtained within 48 h. **^{1}H NMR** (CD_2Cl_2, 25 °C, 300 MHz): δ −0.05 (q, $^3J_{HH}$ = 8.4 Hz, 4H, Al(CH_2CH_3)$_2$), 0.25 (t, $^3J_{HH}$ = 7.9 Hz 6H, Al(CH_2CH_3)$_2$), 2.01 (s, 12H, *o*-Me_{N-Ar}), 2.32 (s, 6H, *p*-Me_{N-Ar}), 2.45 (s, 6H, *Me*−CN), 7.02 (s, 4H, *m*-CH_{N-Ar}), 7.55 (s, 4H, *p*-CH_{Ar} BAr^F_4), 7.73, (br s, 8H, *o*-CH_{Ar} BAr^F_4), 8.45 (d, $^3J_{HH}$ = 7.7 Hz, 2H, 3-CH_{py}), 8.68 (d, $^3J_{HH}$ = 7.8 Hz, 1H, 4-CH_{py}).**^{19}F{^{1}H} NMR** (CD_2Cl_2, 25 °C, 376 MHz): δ −62.85 (s, BAr^F_4).**^{11}B{^{1}H} NMR** (CD_2Cl_2, 25 °C, 128 MHz): δ −6.61 (s, BAr^F_4). **^{13}C{^{1}H} NMR** (CD_2Cl_2, 25 °C, 100 MHz): δ −0.51 (Al(CH_2CH_3)$_2$), 8.23 (Al(CH_2CH_3)$_2$), 17.26 (*Me*−CN), 18.22 (*o*-Me_{N-Ar}), 20.88 (*p*-Me_{N-Ar}), 117.91 (*p*-CH_{Ar} BAr^F_4), 123.66 (CF_3 BAr^F_4), 126.36 (3,5-CH_{Py}), 127.87 (*p*-C_{N-Ar}), 129.30 (q, $^2J_{CF}$ = 33 Hz, *C*-CF_3 BAr^F_4), 130.37 (*m*-CH_{N-Ar}), 135.22

https://doi.org/10.1021/acs.inorgchem.4c02664
Inorg. Chem. 2024, 63, 19156−19166

(o-CH_{Ar} BAr^F_4), 137.99 (o-C_{N-Ar}), 140.04 (i-C_{N-Ar}), 146.98 (4-CH_{Py}), 148.44 (2-CH_{Py}), 162.20 (q, $^1J_{CB}$ = 50 Hz, i-C_{Ar} BAr^F_4), 170.02 (Me−CN). **IR (KBr/Nujol, cm^{-1}):** ν 1599 (intense, C=N, ^{Mes}BIP); 1276, 1125, 887 (B−C for $[BAr^F_4]^-$). **EA for $C_{63}H_{53}AlBF_{24}N_3$** (found vs calculated, bulk sample): C 56.36 (56.22), H 4.16 (3.97), N 3.22 (3.12).

Synthesis of (^{Mes}BIP·)AlEt$_2$ (2d). A J. Young's ampule was loaded with 325 mg (0.241 mmol) of [**1d**][**BAr$^F_4$**] and 46 mg (0.241 mmol) of Cp_2Co. The solids were combined with 3 mL of anhydrous toluene, giving a dark red suspension. This mixture was stirred vigorously at room temperature and progress was monitored via ^{1}H NMR analysis of aliquots. After 4 h, the resonances attributed to [**1d**][**BAr$^F_4$**] disappeared. Subsequent cooling of the mixture to −36 °C initiated the precipitation of [Cp_2Co][BAr^F_4]. The reaction mixture was then filtered into a Schlenk tube via cannula, to which dried n-hexane was added until incipient crystallization occurred, and subsequently stored at −36 °C overnight. The next day, a brown/red solid was collected, isolated by cannula filtration, and dried under vacuum (<10^{-2} mbar) to yield (**^{Mes}BIP·)AlEt$_2$ (2d)** as a red/brown solid. Yield: 70 mg, 0.145 mmol, 60%. Despite the appearance of incipient crystallization, the procedure did not yield single crystals suitable for X-ray diffraction analysis. **Note on ^{1}H NMR data:** *The absence of ^{1}H NMR resonances for (**^{Mes}BIP·)AlEt$_2$ (2d**) is attributable to the paramagnetic nature of the compound.* **EA for $C_{31}H_{41}AlN_3$** (found vs calculated, bulk sample): C 77.33 (77.14), H 8.87 (8.56), N 8.69 (8.71). **IR (KBr/Nujol, cm^{-1}):** ν 1641, 1528 (medium to weak intensity, C=C Py and C=N imine). *The band observed at 1641 cm^{-1} for the C=C stretch is characteristic of the dearomatized pyridine ring.* The **EPR** of **2d** spectrum is available in the Supporting Information.

Redox in Situ NMR Monitoring. General Procedure. Initial Setup. A J. Young tap NMR tube was loaded with 10 mg of the chosen aluminum complex [**$^{Ar'}$BIPAlR$_2$**][**BAr$^F_4$**], (**1a$^+$_d$^+$**, where Ar'= Dipp and Mes and R = Me and Et). Solvents were chosen based on their ability to dissolve the reactants and products, as well as their compatibility with NMR spectroscopy. Depending on the starting complex, either 0.5 mL of CD_2Cl_2 (for complexes with L = ^{Dipp}BIP) or Tol-d_8 (for complexes with L = ^{Mes}BIP) was added. The redox reaction was then in situ monitored via ^{1}H NMR spectroscopy, with continuous monitoring being crucial for determining the exact point of reaction completion and observing the dynamic changes during the redox processes. The temperature was maintained at room temperature to facilitate the redox reactions without additional thermal input.

Reduction Step. Before the addition of the reductant, a ^{1}H NMR experiment was acquired for each aluminum complex **1a$^+$−d$^+$** to establish a baseline. An equimolar quantity of Cp_2Co was then added to the corresponding aluminum complex solution. The solution was mixed using a bespoke NMR tube rotor at room temperature, with the progress and completion of the reduction monitored by ^{1}H NMR analyses. After 20 min, the reduction of all aluminum complexes was confirmed by the disappearance of ^{1}H NMR resonances for **1a$^+$−d$^+$** attributable to the paramagnetic NMR-silence nature of the reduced compound [(**$^{Ar'}$BIP·)AlR$_2$**] (**2a−d**) with the only signals being those of [Cp_2Co][BAr^F_4].

Oxidation Step. Following the reduction of each aluminum complex to the corresponding **2a−d**, species, an equimolar amount of [Fc][PF_6] was added. The mixture was then mixed and monitored by ^{1}H NMR analyses. After 20 min, the oxidation of the aluminum species was evidenced by the reappearance of ^{1}H NMR resonances for the species **1a$^+$−d$^+$** along with resonances attributable to Fc and species [Cp_2Co]$^+$.

Notes on Alternative Reducing and Oxidizing Agents. Further experiments tested the redox behavior using Ferrocene (Fc) and Cp_2Co as alternative reducing agents, with only Cp_2Co successfully reducing the aluminum complexes **1a$^+$−d$^+$**. Attempts to oxidize the **2a−d** species with [Fc][BF_4] failed. THF-d_8 was also trialed as a solvent; however, it led to degradation of the reduced aluminum species, resulting in complex reaction mixtures.

Single-Crystal X-ray Analysis. A summary of the crystallographic data and the structure refinement results for compounds [**1a**][**BAr$^F_4$**], [**1c**][PF_6], [**1d**][**BAr$^F_4$**], [**Cp$_2$Co**][**BAr$^F_4$**] and **2b** is given in Tables S1−S5 in the Supporting Information. Crystals of a suitable size for X-ray diffraction analysis were coated with dry perfluoropolyether and mounted on glass fibers and fixed in a cold nitrogen stream (T = 193 K) to the goniometer head. Data collection was carried out on a Bruker-AXS, D8 QUEST ECO, PHOTON II area detector diffractometer, using monochromatic radiation λ(Mo K_α) = 0.71073 Å, by means of ω and φ scans with a width of 0.50°. The data were reduced (SAINT[34]) and corrected for absorption effects by the multiscan method (SADABS[35]). The structures were solved by intrinsic phasing modification of direct methods (SHELXT[36]) and refined against all F^2 data by full-matrix least-squares techniques (SHELXL-2018/3[37]) minimizing $w[F_o^2 - F_c^2]^2$. All non-hydrogen atoms were refined anisotropically. The hydrogen atoms were included from calculated positions and refined riding on their respective carbon atoms with isotropic displacement parameters. In general, the $-CF_3$ groups of BAr^F_4 in [**1a**][**BAr$^F_4$**] present positional disorder, so five of them were modeled as two components of the disorder with their respective occupancy coefficients. Therefore, it was also necessary to use some geometric restraints (SADI, SIMU) during the structure refinement to ensure a sensible geometry. In the asymmetric unit of [**1c**][PF_6], a crystallizing THF molecule that did not need to be modeled is shown next to the salt complex. A search for solvent-accessible voids for structure [**1a**]-[**BAr$^F_4$**] using SQUEEZE[38] showed two volumes of potential solvents of 190 Å^3 for each (52 electron count), whose solvent content could not be identified or refined with the most severe restrictions, but due to the volume and the electrons present, it would match a very disordered n-hexane molecule. While a search for solvent-accessible voids for the [**1c**][PF_6] structure using SQUEEZE showed a single potential solvent volume of 292 Å3 (70 electron count), whose solvent content could not be identified or refined under the most severe constraints, but due to the volume and electrons present, it would match one and a half molecules of very disordered n-hexane. The corresponding CIF data represent SQUEEZE treated structures with the solvent molecules handling as a diffuse contribution to the overall scattering, without specific atom position and excluded from the structural model. The SQUEEZE results were appended to the CIF. Crystallizing compounds [**1a**][**BAr$^F_4$**] and [**1c**][PF_6] is challenging due to their instability, and they appear somewhat twinned, exhibiting at least four additional minority domains. Refining these structures using HKLF 5 and BASF did not yield improved results. Consequently, due to the imperfections in the crystals and the presence of some disorder, as previously discussed and resolved, all the R-values are somewhat elevated. Single-crystal X-ray diffraction data for [**Cp$_2$Co**][**BAr$^F_4$**] and **2b** were obtained under a nitrogen gas stream using an Oxford Cryostream 800 unit[39] at the specified temperature with a Bruker D8 Quest Eco diffractometer equipped with a Photon II 7 detector (Mo, λ = 0.71073 Å). The raw frame data was reduced using APEX3. Structures were resolved using SHELXT and refined using full-matrix least-squares refinement on all F^2 data using the SHELXL[40] interface within GUI OLEX2.[41] Unless stated otherwise, all non-hydrogen atoms were refined anisotropically, while hydrogen atoms were geometrically placed and allowed to ride on their parent atoms. Disorder was addressed by implementing a split-site model and restraining geometries and displacement parameters. In several structures some of the CF_3 groups on the $BAr^F_4{}^-$ anion was disordered and modeled over two main domains, and restrained to maintain sensible geometries. Distances and angles were calculated using the full covariance matrix. The corresponding crystallographic data were deposited with the Cambridge Crystallographic Data Centre as supplementary publications. CCDC 2337930 ([**1a**]-[**BAr$^F_4$**]), 2337931 ([**1c**][PF_6]), 2334613 ([**1d**][**BAr$^F_4$**]) 2326416 [**Cp$_2$Co**][**BAr$^F_4$**] and 2326417 for **2b** contain the supplementary crystallographic data for this paper. The data can be obtained free of charge via: https://www.ccdc.cam.ac.uk/structures/.

https://doi.org/10.1021/acs.inorgchem.4c02664
Inorg. Chem. 2024, 63, 19156−19166

■ ASSOCIATED CONTENT

Supporting Information

The Supporting Information is available free of charge at https://pubs.acs.org/doi/10.1021/acs.inorgchem.4c02664.

Instrumentation description, characterization data including NMR, IR and EPR spectra, EA, crystallographic files (CIF), cyclic voltammetry (CV), and computational data (PDF)

Accession Codes

Accession Codes. CCDC 2337930, 2337931, 2334613, 2326416 and 2326417 contain the supplementary crystallographic data for this paper. This data can be obtained free of charge via www.ccdc.cam.uk/data_request/cif or by emailing data_request@ccdc.cam.uk or by contacting the Cambridge Crystallographic Data Centre 12, Union Road, Cambridge CB2 IEZ, UK; fax +44 1223 336033.

■ AUTHOR INFORMATION

Corresponding Authors

Antonio J. Martínez-Martínez − *CIQSO-Center for Research in Sustainable Chemistry and Department of Chemistry, CSIC-Associated Unit, University of Huelva, Huelva 21007, Spain;* orcid.org/0000-0002-0684-1244; Email: antonio.martinez@dqcm.uhu.es

Antonio Rodríguez-Delgado − *Instituto de Investigaciones Químicas, CSIC-Universidad de Sevilla, Sevilla 41092, Spain;* orcid.org/0000-0002-2207-9149; Email: arodriguez@us.es

Juan Cámpora − *Instituto de Investigaciones Químicas, CSIC-Universidad de Sevilla, Sevilla 41092, Spain;* orcid.org/0000-0001-7305-1296; Email: campora@iiq.csic.es

Authors

Juan Manuel Delgado-Collado − *Instituto de Investigaciones Químicas, CSIC-Universidad de Sevilla, Sevilla 41092, Spain;* orcid.org/0009-0006-2000-9303

Hellen Videa − *CIQSO-Center for Research in Sustainable Chemistry and Department of Chemistry, CSIC-Associated Unit, University of Huelva, Huelva 21007, Spain;* orcid.org/0000-0002-8171-9804

Pablo J. Serrano-Laguna − *CIQSO-Center for Research in Sustainable Chemistry and Department of Chemistry, CSIC-Associated Unit, University of Huelva, Huelva 21007, Spain;* orcid.org/0000-0003-0567-5587

M. Ángeles Fuentes − *CIQSO-Center for Research in Sustainable Chemistry and Department of Chemistry, CSIC-Associated Unit, University of Huelva, Huelva 21007, Spain;* orcid.org/0000-0003-4546-3984

Eleuterio Álvarez − *Instituto de Investigaciones Químicas, CSIC-Universidad de Sevilla, Sevilla 41092, Spain;* orcid.org/0000-0002-8378-8459

Antonio Díaz Quintana − *Instituto de Investigaciones Químicas, CSIC-Universidad de Sevilla, Sevilla 41092, Spain;* orcid.org/0000-0001-8973-8009

Complete contact information is available at: https://pubs.acs.org/10.1021/acs.inorgchem.4c02664

Author Contributions

[§]J.M.D.-C., H.V., and P.J.S.-L. authors contributed equally. The manuscript was written through contributions of all authors. All authors have given approval to the final version of the manuscript.

Notes

The authors declare no competing financial interest.

■ ACKNOWLEDGMENTS

The authors acknowledge the financial support by the Ministerio de Ciencia e Innovación MICIN/AEI/10.13039/501100011033 (grants PID2021-128392NB-100 for J.C., PID2019-108292RA-I00 and PID2022-142270OB-I00 for A.J.M.-M.) and MICIN/NextGenerationEU/PRTR (CNS2022-136087 for A.J.M.-M), the Thematic Network "OASIS" RED2022-134074-T, the ERDF/EU, the Junta de Andalucía (grant P20_00104 for J.C. and P20_00373 for A.J.M.-M.) and the University of Huelva (UHU-202043 and EPIT1442023 for A.J.M.-M.). A.J.M.-M. also thanks the Spanish Research State Agency AEI for a Ramón y Cajal research (RYC-2017-21783).

■ REFERENCES

(1) 5th Chemical Sciences and Society Summit (CS3) 2013 Whitepaper: Efficient Utilization of Elements. 2013, https://www.acs.org/content/dam/acsorg/greenchemistry/industriainnovation/cs3-whitepaper2013.pdf. (b) Hunt, A. Element Recovery and Sustainability. In *Green Chemistry*; Clark, J. H., Ed.; RSC Publishing: Cambridge,CB4 0WF, UK, 2013; p 270. (c) Hunt, A. J.; Matharu, A. S.; King, A. H.; Clark, J. H. The importance of elemental sustainability and critical element recovery. *Green Chem.* **2015**, *17*, 1949−1950. (d) Rhodes, C. J. Endangered elements, critical raw materials and conflict minerals. *Sci. Prog.* **2019**, *102*, 304−350.

(2) (a) Wheelhouse, K. M. P.; Webster, R. L.; Beutner, G. L. Advances and Applications in Catalysis with Earth-Abundant Metals. *Organometallics* **2023**, *42*, 1677−1679. (b) Fürstner, A. Iron Catalysis in Organic Synthesis: A Critical Assessment of What It Takes To Make This Base Metal a Multitasking Champion. *ACS Central Sci.* **2016**, *2*, 778−789. (c) Chirik, P. J.; Morris, R. Getting Down to Earth: The Renaissance of Catalysis with Abundant Metals. *Acc. Chem. Res.* **2015**, *48*, 2495. (d) Bullock, M. *Catalysis without Precious Metals*; Wiley-VCH, 2010. (e) Phapale, V. B.; Cárdenas, D. J. Nickel-catalysed Negishi cross-coupling reactions: scope and mechanisms. *Chem. Soc. Rev.* **2009**, *38*, 1598−1607.

(3) Holland, P. L. Distinctive Reaction Pathways at Base Metals in High-Spin Organometallic Catalysts. *Acc. Chem. Res.* **2015**, *48*, 1696−1702.

(4) Bullock, R. M.; Chen, J. G.; Gagliardi, L.; Chirik, P. J.; Farha, O. K.; Hendon, C. H.; Jones, C. W.; Keith, J. A.; Klosin, J.; Minteer, S. D.; et al. Using nature's blueprint to expand catalysis with Earth-abundant metals. *Science* **2020**, *369*, No. eabc3183.

(5) (a) Khusnutdinova, J. R.; Milstein, D. Metal−Ligand Cooperation. *Angew. Chem., Int. Ed.* **2015**, *54*, 12236−12273. (b) Wodrich, M. D.; Hu, X. Natural inspirations for metal-ligand cooperative catalysis. *Nat. Rev. Chem* **2017**, *2*, 0099−107. (c) Baumgardner, D. F.; Parks, W. E.; Gilbertson, J. D. Harnessing the active site triad: merging hemilability, proton responsivity, and ligand-based redox-activity. *Dalton Trans.* **2020**, *49*, 960−965. (d) Elsby, M. R.; Baker, R. T. Strategies and mechanisms of metal−ligand cooperativity in first-row transition metal complex catalysts. *Chem. Soc. Rev.* **2020**, *49*, 8933−8987.

(6) (a) Sterle, M.; Huš, M.; Lozinšek, M.; Zega, A.; Cotman, A. E. Hydrogen-Bonding Ability of Noyori−Ikariya Catalysts Enables Stereoselective Access to CF3-Substituted syn-1,2-Diols via Dynamic Kinetic Resolution. *ACS Catal.* **2023**, *13*, 6242−6248. (b) Lan, S.; Huang, H.; Liu, W.; Xu, C.; Lei, X.; Dong, W.; Liu, J.; Yang, S.; Cotman, A. E.; Zhang, Q.; et al. Asymmetric Transfer Hydrogenation of Cyclobutenediones. *J. Am. Chem. Soc.* **2024**, *146*, 4942−4957.

(7) (a) Luca, O. R.; Crabtree, R. H. Redox-active ligands in catalysis. *Chem. Soc. Rev.* **2013**, *42*, 1440−1459. (b) Blanchard, S.; Derat, E.; Desage-El Murr, M.; Fensterbank, L.; Malacria, M.; Mouriès-Mansuy, V. Non-Innocent Ligands: New Opportunities in Iron Catalysis. *Eur.*

J. Inorg. Chem. **2012**, *2012*, 376−389. (c) Chacon-Teran, M. A.; Findlater, M. Redox-Active BIAN-Based Iron Complexes in Catalysis. *Eur. J. Inorg. Chem.* **2022**, *2022*, No. e202200363. (d) Swatiputra, A. A.; Mukherjee, D.; Dinda, S.; Roy, S.; Pramanik, K.; Ganguly, S. Electron transfer catalysis mediated by 3d complexes of redox non-innocent ligands possessing an azo function: a perspective. *Dalton Trans.* **2023**, *52*, 15627−15646. (e) Protchenko, A. V.; Dange, D.; Harmer, J. R.; Tang, C. Y.; Schwarz, A. D.; Kelly, M. J.; Phillips, N.; Tirfoin, R.; Birjkumar, K. H.; Jones, C.; Kaltsoyannis, N.; Mountford, P.; et al. Stable GaX_2, InX_2 and TlX_2 radicals. *Nat. Chem.* **2014**, *6*, 315−319. (f) Regenauer, N. I.; Wadepohl, H.; Roşca, D. A. Metal−Ligand Cooperativity in Iron Dinitrogen Complexes: Proton-Coupled Electron Transfer Disproportionation and an Anionic $Fe(0)N_2$ Hydride. *Inorg. Chem.* **2022**, *61* (19), 7426−7435.

(8) (a) Berben, L. A. Catalysis by Aluminum (III) Complexes of Non-Innocent Ligands. *Chem.—Eur. J.* **2015**, *21*, 2734−2742. (b) Parsons, L. W. T.; Berben, L. A. Metallated dihydropyridinates: prospects in hydride transfer and (electro)catalysis. *Chem. Sci.* **2023**, *14*, 8234−8248. (c) Carr, C. R.; Vesto, J. I.; Xing, X.; Fettinger, J. C.; Berben, L. A. Aluminum-Ligand Cooperative O−H Bond Activation Initiates Catalytic Transfer Hydrogenation. *ChemCatChem* **2022**, *14* (13), 202101869. (d) Gahlaut, P. S.; Yadal, K.; Gautam, D.; Jana, B. Recent Development in the Syntheses of Aluminum Complexes Based on Redox-Active Ligands. *J. Organomet. Chem.* **2022**, *963*, 122298.

(9) (a) Cámpora, J.; Rodríguez-Delgado, A.; Palma, P. σ-Organometallic Chemistry With 2,6-Bis(imino) pyridine Ligands: New Pathways to Innovative Pincer Architectures. In *Pincer Compounds: Chemistry and Applications*; Morales-Morales; Ed.; Wiley: Amsterdam, 2018; pp 539−586. (b) Zhu, D.; Thapa, I.; Korobkov, I.; Gambarotta, S.; Budzelaar, P. H. M. Redox-Active Ligands and Organic Radical Chemistry. *Inorg. Chem.* **2011**, *50*, 9879−9887. (c) Römelt, C.; Weyhermüller, T.; Wieghardt, K. Structural characteristics of redox-active pyridine-1,6-diimine complexes: Electronic structures and ligand oxidation levels. *Coord. Chem. Rev.* **2019**, *380*, 287−317.

(10) (a) Flisak, Z.; Sun, W.-H. Progression of Diiminopyridines: From Single Application to Catalytic Versatility. *ACS Catal.* **2015**, *5*, 4713−4724. (b) Small, B. L. Discovery and Development of Pyridine-bis(imine) and Related Catalysts for Olefin Polymerization and Oligomerization. *Acc. Chem. Res.* **2015**, *48*, 2599−2611.

(11) Chirik, P. J.; Wieghardt, K. Radical Ligands Confer Nobility on Base-Metal Catalysts. *Science* **2010**, *327*, 794−795.

(12) Chirik, P. J. Carbon−Carbon Bond Formation in a Weak Ligand Field: Leveraging Open-Shell First-Row Transition-Metal Catalysts. *Angew. Chem., Int. Ed.* **2017**, *56*, 5170−5181.

(13) Chirik, P. J. Iron- and Cobalt-Catalyzed Alkene Hydrogenation: Catalysis with Both Redox-Active and Strong Field Ligands. *Acc. Chem. Res.* **2015**, *48*, 1687−1695.

(14) (a) de Almeida, L. D.; Wang, H. L.; Junge, K.; Cui, X. J.; Beller, M. Recent Advances in Catalytic Hydrosilylations: Developments beyond Traditional Platinum Catalysts. *Angew. Chem., Int. Ed.* **2021**, *60*, 550−565. (b) Royo, B. Recent advances in catalytic hydrosilylation of carbonyl groups mediated by well-defined first-row late transition metals. In *Advances in Organometallic Chemistry*; Pérez, P. J., Ed.; Academic Press, 2019; Vol. *72*, pp 59−102.

(15) Obligacion, J. V.; Neely, J. M.; Yazdani, A. N.; Pappas, I.; Chirik, P. J. Cobalt Catalyzed Z-Selective Hydroboration of Terminal Alkynes and Elucidation of the Origin of Selectivity. *J. Am. Chem. Soc.* **2015**, *137*, 5855−5858.

(16) Scott, J.; Gambarotta, S.; Korobkov, I.; Knijnenburg, Q.; de Bruin, B.; Budzelaar, P. H. M. Formation of a Paramagnetic Al Complex and Extrusion of Fe during the Reaction of (Diiminepyridine)Fe with AlR_3 (R = Me, Et). *J. Am. Chem. Soc.* **2005**, *127*, 17204−17206.

(17) Cartes, M. A.; Rodríguez-Delgado, A.; Palma, P.; Álvarez, E.; Cámpora, J. Sequential Reduction and Alkyl Exchange Reactions of Bis(imino)pyridine Dialkyliron(II) with Trimethylaluminum. *Organometallics* **2014**, *33*, 1834−1839.

(18) Dabringhaus, P.; Heizmann, T.; Krossing, I. Activation of the GaI Cation for Bond Activation: from Oxidative Additions into C−Cl and H−P Bonds to Reversible Insertion into P4. *Chem.—Eur. J.* **2023**, *29*, No. e202302212.

(19) See, for example: (a) Dawkins, M. J. C.; Simonov, A. N.; Jones, C. 2,6-Diiminopyridine complexes of group 2 metals: synthesis, characterisation and redox behaviour. *Dalton Trans.* **2020**, *49*, 6627−6634. (b) Chu, T.; Belding, L.; Poddutoori, P. K.; van der Est, A.; Dudding, T.; Korobkov, I.; Nikonov, G. I. Unique molecular geometries of reduced 4- and 5-coordinate zinc complexes stabilised by diiminopyridine ligand. *Dalton Trans.* **2016**, *45*, 13440−13448. (c) Chu, T.; Belding, L.; van der Est, A.; Dudding, T.; Korobkov, I.; Nikonov, G. I. A Coordination Compound of Ge0 Stabilized by a Diiminopyridine Ligand. *Angew. Chem., Int. Ed.* **2014**, *53*, 2711−2715.

(20) Myers, T. W.; Berben, L. A. Aluminum−Ligand Cooperative N−H Bond Activation and an Example of Dehydrogenative Coupling. *J. Am. Chem. Soc.* **2013**, *135*, 9988−9990.

(21) Thompson, E. J.; Myers, T. W.; Berben, L. A. Synthesis of Square-Planar Aluminum(III) Complexes. *Angew. Chem., Int. Ed.* **2014**, *53*, 14132−14134.

(22) Myers, T. W.; Sherbow, T. J.; Fettinger, J. C.; Berben, L. A. Synthesis and characterization of bis(imino)pyridine complexes of divalent Mg and Zn. *Dalton Trans.* **2016**, *45*, 5989−5998.

(23) Pérez, C. M.; Rodríguez-Delgado, A.; Palma, P.; Álvarez, E.; Gutiérrez-Puebla, E.; Cámpora, J. Neutral and Cationic Alkylmanganese(II) Complexes Containing 2,6-Bisiminopyridine Ligands. *Chem.—Eur. J.* **2010**, *16*, 13834−13842.

(24) Sandoval, J. J.; Álvarez, E.; Palma, P.; Rodríguez-Delgado, A.; Cámpora, J. Neutral Bis(imino)-1,4-dihydropyridinate and Cationic Bis(imino)pyridine σ-Alkylzinc(II) Complexes as Hydride Exchange Systems: Classic Organometallic Chemistry Meets Ligand-Centered, Biomimetic Reactivity. *Organometallics* **2018**, *37*, 1734−1744.

(25) (a) Knijnenburg, Q.; Gambarotta, S.; Budzelaar, P. H. M. Ligand-centred reactivity in diiminepyridine complexes. *Dalton Trans.* **2006**, 5442−5448. (b) Budzelaar, P. H. M.; de Bruin, B.; Gal, A. W.; Wieghardt, K.; van Lenthe, J. H. Metal-to-Ligand Electron Transfer in Diiminopyridine Complexes of Mn−Zn. A Theoretical Study. *Inorg. Chem.* **2001**, *40*, 4649−4655.

(26) Cámpora, J.; Naz, A. M.; Palma, P.; Álvarez, E.; Reyes, M. L. 2,6-Diiminopyridine Iron(II) Dialkyl Complexes. Interaction with Aluminum Alkyls and Ethylene Polymerization Catalysis. *Organometallics* **2005**, *24*, 4878−4881.

(27) Sandoval, J. J.; Palma, P.; Álvarez, E.; Rodríguez-Delgado, A.; Cámpora, J. Dibenzyl and diallyl 2,6-bisiminopyridinezinc(ii) complexes: selective alkyl migration to the pyridine ring leads to remarkably stable dihydropyridinates. *Chem. Commun.* **2013**, *49*, 6791−6793.

(28) Connelly, N. G.; Geiger, W. E. Chemical Redox Agents for Organometallic Chemistry. *Chem. Rev.* **1996**, *96*, 877−910.

(29) For complexes **2**, in addition to **2b** we used literature data for **2a** and **2c** (see refs 16 and 17, respectively).

(30) The NC-C(Py), C=N and αC−N(Py) bond distances for $\mathbf{1}^+$ and **2** can be used to calculate the corresponding Δgeometry parameters, which correlate with the reduction state of the BIP ligand (see ref 9c). Theoretically calculated (DFT-based) values of Δf or the neutral and singly reduced BIP ligands are 0.184 and 0.120, respectively. The average Δf or $\mathbf{1}^+$ and **2** are 0.17 ± 0.05 and 0.10 ± 0.06, respectively (error intervals taken $\approx 3\sigma$), respectively.

(31) (a) Budzelaar, P. H. M. Radical Chemistry of Iminepyridine Ligands. *Eur. J. Inorg. Chem.* **2012**, *2012*, 530−534. (b) Sherbow, T. J.; Parsons, L. W. T.; Phan, N. A.; Fettinger, J. C.; Berben, L. A. Ligand Conjugation Directs the Formation of a 1,3-Dihydropyridinate Regioisomer. *Inorg. Chem.* **2020**, *59*, 17614−17619.

(32) Toma, M.; Kuvek, T.; Vrček, V. Ionization Energy and Reduction Potential in Ferrocene Derivatives: Comparison of Hybrid and Pure DFT Functionals. *J. Phys. Chem. A* **2020**, *124*, 8029−8039.

(33) Blackman, A. G.; Schenk, E. B.; Jelley, R. E.; Krenske, E. H.; Gahan, L. R. Five-coordinate transition metal complexes and the value of τ5: observations and caveats. *Dalton Trans.* **2020**, *49*, 14798−14806.

https://doi.org/10.1021/acs.inorgchem.4c02664
Inorg. Chem. 2024, 63, 19156−19166

(34) *Bruker, SAINT+*; Bruker AXS Inc.: Madison, Wisconsin, USA, 2007.
(35) Sheldrick, G. M. *SADABS, Programs Scaling Absorpt. Correct. Area Detect. Data*; University of Göttingen: Göttingen, Germany, 1997.
(36) Sheldrick, G. SHELXT - Integrated space-group and crystal-structure determination. *Acta Crystallogr., Sect. A* **2015**, *71*, 3−8.
(37) Sheldrick, G. Crystal structure refinement with SHELXL. *Acta Crystallogr., Sect. C: Struct. Chem.* **2015**, *71*, 3−8.
(38) van der Sluis, P.; Spek, A. L. BYPASS: an effective method for the refinement of crystal structures containing disordered solvent regions. *Acta Crystallogr., Sect. A* **1990**, *46*, 194−201.
(39) Cosier, J.; Glazer, A. M. A nitrogen-gas-stream cryostat for general X-ray diffraction studies. *J. Appl. Crystallogr.* **1986**, *19*, 105−107.
(40) Sheldrick, G. A short history of SHELX. *Acta Crystallogr., Sect. A* **2008**, *64*, 112−122.
(41) Dolomanov, O. V.; Bourhis, L. J.; Gildea, R. J.; Howard, J. A. K.; Puschmann, H. OLEX2: a complete structure solution, refinement and analysis program. *J. Appl. Crystallogr.* **2009**, *42*, 339−341.

https://doi.org/10.1021/acs.inorgchem.4c02664
Inorg. Chem. 2024, 63, 19156−19166